

Optical Spectral Singularities and Coherent Perfect Absorption in a Two-Layer Spherical Medium

Ali Mostafazadeh* and Mustafa Sarısamam†
 Department of Mathematics, Koç University,
 34450 Sarıyer, Istanbul, Turkey

Abstract

An optical spectral singularity is a zero-width resonance that corresponds to lasing at threshold gain. Its time-reversal causes coherent perfect absorption of light and forms the theoretical basis of antilasing. In this article we explore optical spectral singularities of a two-layer spherical medium. In particular, we examine the cases that a gain medium is coated by a thin layer of high-refractive index glass and a spherical glass covered by a layer of gain material. In the former case, the coating reduces the minimum radius required for exciting spectral singularities and gives rise to the formation of clusters of spectral singularities separated by wide spectral gaps. In the latter case, the coating leads to a doubling of the number of spectral singularities.

PACS numbers: 03.65.Nk, 42.25.Bs, 42.60.Da, 24.30.Gd

Keywords: Complex potential, spectral singularity, zero-width resonance, gain medium, coated spherical dye laser, coherent perfect absorption, antilaser

1 Introduction

The discovery [1] that the mathematical concept of a spectral singularity [2] has physical realizations as zero-width resonances of complex scattering potentials has motivated a detailed study of this phenomenon [3] – [12]. In particular, it is shown that optical spectral singularities (OSS) correspond to the lasing at the threshold gain [8] and that a time-reversed optical spectral singularity [7] yields a coherent perfect absorption (CPA) of light, i.e., an antilaser [13].

Typical lasers are photonic devices consisting of an active medium placed inside an optical cavity. A particularly interesting type of lasers are those based on spherical granules where the surface of the sphere acts as the cavity [14]. These are characterized by their extremely high quality factors and small volumes of excitation. Owing to these properties, a spherical laser can also be realized in which the active medium is located outside an spherical core [15].

In Ref. [11] we studied the OSS of a uniform spherical gain medium and showed for the radial (transverse) modes of a concrete spherical dye laser that the emergence of an OSS puts a lower bound on the radius of the gain medium. This is the minimum radius $a^{(\min)}$ required for lasing in these modes. In the present article we examine OSS and CPA for an active medium consisting of a spherical inner core and a spherical outer shell with different refractive indices, as shown in Figure 1. In particular, we wish to explore the prospects of reducing the value of $a^{(\min)}$ by means of coating the spherical gain medium by a material with higher refractive index.¹

*E-mail address: amostafazadeh@ku.edu.tr, Phone: +90 212 338 1462, Fax: +90 212 338 1559

†E-mail address: msarisaman@ku.edu.tr, Phone: +90 212 338 1378, Fax: +90 212 338 1559

¹It is well-known that the presence of such a coating increases the system's quality factor [15, 16].

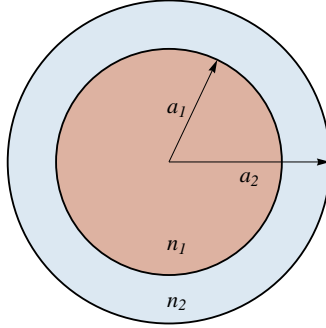


Figure 1: (Color online) Two-layer spherical gain medium. a_1 and a_2 are the inner and outer radii of the spherical shell; \mathbf{n}_1 and \mathbf{n}_2 are the complex refractive indices of the inner core and the outer shell, respectively.

2 Radial Transverse Spherical Electromagnetic Waves

Consider an optically active material with an inner spherical core of radius a_1 and an outer spherical shell of thickness $a_2 - a_1$ placed in vacuum. Let \mathbf{n}_1 and \mathbf{n}_2 denote the complex refractive indices of the inner core and the outer shell, respectively, and suppose that they are independent of space and time. The electromagnetic (EM) waves interacting with this system satisfy the Maxwell equations:

$$\vec{\nabla} \cdot \vec{D} = 0, \quad \vec{\nabla} \cdot \vec{B} = 0, \quad (1)$$

$$\vec{\nabla} \times \vec{E} + \dot{\vec{B}} = 0, \quad \vec{\nabla} \times \vec{H} - \dot{\vec{D}} = 0, \quad (2)$$

where $\vec{D} := \varepsilon_0 \mathfrak{z}(r) \vec{E}$, $\vec{H} := \mu_0^{-1} \vec{B}$, ε_0 and μ_0 are respectively the permeability and permittivity of the vacuum, $r := |\vec{r}|$ is the radial spherical coordinate,

$$\mathfrak{z}(r) := \begin{cases} \mathbf{n}_1^2 & \text{for } r < a_1, \\ \mathbf{n}_2^2 & \text{for } a_1 \leq r < a_2, \\ 1 & \text{for } r \geq a_2, \end{cases} \quad (3)$$

and each over-dot represents a time-derivative. According to (2), the electric field $\vec{E} = \vec{E}(\vec{r}, t)$ is a solution of the wave equation:

$$\ddot{\vec{E}}(\vec{r}, t) + \Omega^2 \vec{E}(\vec{r}, t) = 0, \quad r \neq a_1, a_2, \quad (4)$$

where $\Omega^2 := c^2 \mathfrak{z}(r)^{-1} \vec{\nabla} \times \vec{\nabla} \times$ and $c = (\varepsilon_0 \mu_0)^{-1/2}$ is the speed of light in vacuum.

For a time-harmonic EM field with angular frequency ω that propagates in a charge-free medium, we have $\vec{E}(\vec{r}, t) = e^{-i\omega t} \vec{E}(\vec{r})$, and (4) reduces to the time-independent Schrödinger equation:

$$-\nabla^2 \vec{E}(\vec{r}) + v(r) \vec{E}(\vec{r}) = k^2 \vec{E}(\vec{r}), \quad (5)$$

where $k := \omega/c$ is the wave number and v is the complex barrier potential: $v(r) := k^2 [1 - \mathfrak{z}(r)]$.²

Following the analysis of Ref. [11], we investigate transverse radially propagating spherical solutions of (5) that have the form

$$\vec{E}(\vec{r}) = E(r) \hat{\phi}. \quad (6)$$

²Note that (5) is nothing but the well-known Helmholtz equation, and the potential appearing in it is energy-dependent. For the purposes of our investigation this does not cause any difficulty.

Here $\hat{\phi}$ is the unit vector associated with the azimuthal angular coordinate ϕ of the spherical coordinate system. Inserting (6) in (5) yields

$$\left[\frac{d^2}{dr^2} + \frac{2}{r} \frac{d}{dr} + k^2 - v(r) - \frac{1}{r^2} \right] E(r) = 0. \quad (7)$$

For $r < a_1$, $a_1 < r < a_2$ and $r > a_2$ where v takes constant values, we can transform (7) to the spherical Bessel equation of order $\nu := \frac{\sqrt{5}}{2}$, [17]. Therefore,

$$E(r) = \begin{cases} A_1 j_\nu(k_1 r) + B_1 n_\nu(k_1 r) & \text{for } r < a_1, \\ A_2 j_\nu(k_2 r) + B_2 n_\nu(k_2 r) & \text{for } a_1 < r < a_2, \\ A_3 h_\nu^{(1)}(kr) + B_3 h_\nu^{(2)}(kr) & \text{for } r > a_2, \end{cases} \quad (8)$$

where the A_i and B_i are constant numerical coefficients, j_ν, n_ν and $h_\nu^{(i)}$ are respectively the spherical Bessel, Neumann, and Hankel functions, and $k_i := \mathbf{n}_i k$ for $i = 1, 2$. Notice that the condition that the electric field be regular at the origin implies that $B_1 = 0$. Consequently, $E(0) = 0$.

Having obtained the explicit form of the electric field, we can compute the magnetic field using (2). This gives

$$\vec{B}(\vec{r}, t) = e^{-i\omega t} B(r) \hat{\theta}, \quad (9)$$

where $\hat{\theta}$ is the unit vector associated with the spherical polar coordinate θ ,

$$B(r) := i\omega^{-1} \tilde{E}(r) = \begin{cases} i\omega^{-1} [A_1 \tilde{j}_\nu(k_1 r) + B_1 \tilde{n}_\nu(k_1 r)] & \text{for } r < a_1, \\ i\omega^{-1} [A_2 \tilde{j}_\nu(k_2 r) + B_2 \tilde{n}_\nu(k_2 r)] & \text{for } a_1 < r < a_2, \\ i\omega^{-1} [A_3 \tilde{h}_\nu^{(1)}(kr) + B_3 \tilde{h}_\nu^{(2)}(kr)] & \text{for } r > a_2, \end{cases} \quad (10)$$

and for each differentiable function f we define \tilde{f} according to $\tilde{f}(r) := \left(\frac{d}{dr} + \frac{1}{r} \right) f(r)$. Notice that for every pair of differentiable functions $f, g : \mathbb{R}^+ \rightarrow \mathbb{R}$ and positive real numbers $r, s \in \mathbb{R}^+$,

$$f(r)\tilde{g}(s) - g(s)\tilde{f}(r) = f(r)g'(s) - g(s)f'(r). \quad (11)$$

Because this quantity will frequently appear in our calculations, we denote it by $f(r) \overleftrightarrow{\partial} g(s)$ for brevity. In other words,

$$f(r) \overleftrightarrow{\partial} g(s) := f(r)g'(s) - g(s)f'(r) = f(r)\tilde{g}(s) - g(s)\tilde{f}(r). \quad (12)$$

Recall that the Wronskian of f and g is given by $W[f(r), g(r)] := f(r) \overleftrightarrow{\partial} g(r)$. Therefore

$$f(r)\tilde{g}(r) - g(r)\tilde{f}(r) = W[f(r), g(r)]. \quad (13)$$

In order to relate the coefficients A_j and B_j appearing in (8), we need to impose the appropriate matching conditions at the boundaries $r = a_1$ and $r = a_2$, [17]. For the system we consider, these correspond to the condition that the parallel component of both the electric and magnetic fields must be continuous at the boundaries. In view of (6) and (9), this means that $E = E(r)$ and $B = B(r)$ must be continuous functions. We can satisfy this condition provided that we select the coefficients A_i and B_i such that E and B are continuous at $r = a_1$ and $r = a_2$. This gives

$$\mathbf{K}_{11} \begin{bmatrix} A_1 \\ 0 \end{bmatrix} = \mathbf{K}_{12} \begin{bmatrix} A_2 \\ B_2 \end{bmatrix}, \quad \mathbf{K}_{22} \begin{bmatrix} A_2 \\ B_2 \end{bmatrix} = \mathbf{L} \begin{bmatrix} A_3 \\ B_3 \end{bmatrix}, \quad (14)$$

where for all $p, q = 1, 2$,

$$\mathbf{K}_{pq} := \begin{bmatrix} j_\nu(k_q a_p) & n_\nu(k_q a_p) \\ \tilde{j}_\nu(k_q a_p) & \tilde{n}_\nu(k_q a_p) \end{bmatrix}, \quad \mathbf{L} := \begin{bmatrix} h_\nu^{(1)}(ka_2) & h_\nu^{(2)}(ka_2) \\ \tilde{h}_\nu^{(1)}(ka_2) & \tilde{h}_\nu^{(2)}(ka_2) \end{bmatrix}. \quad (15)$$

According to these equations and (13),

$$\det(\mathbf{K}_{pq}) = W[j_\nu(x), n_\nu(x)] \Big|_{x=k_q a_p} = (k_q a_p)^{-2} \neq 0, \quad (16)$$

$$\det(\mathbf{L}) = W[h_\nu^{(1)}(x), h_\nu^{(2)}(x)] \Big|_{x=ka_2} = -i(ka_2)^{-2} \neq 0. \quad (17)$$

The fact that these quantities do not vanish was to be expected, because (j_ν, n_ν) and $(h^{(1)}, h^{(2)})$ are pairs of linearly-independent solutions of a second order homogeneous linear differential equation. Eqs. (16) and (17) imply that \mathbf{K}_{pq} and \mathbf{L} are invertible matrices. We can use their inverse together with Eq. (14) and the fact that $A_1 \neq 0$, to express A_3 and B_3 in terms of A_1 according to $A_3 = M_{11}A_1$ and $B_3 = M_{21}A_1$, where M_{ij} are the entries of the transfer matrix

$$\mathbf{M} := \mathbf{L}^{-1} \mathbf{K}_{22} \mathbf{K}_{12}^{-1} \mathbf{K}_{11}. \quad (18)$$

3 OSS and CPA for Radial Transverse Spherical Waves

As discussed in Ref. [11], we can easily exploit the asymptotic properties of the spherical Hankel functions to infer that the reflection amplitude of our system is given by

$$R := \frac{A_3}{B_3} = \frac{M_{11}}{M_{21}}. \quad (19)$$

Therefore, in order for characterizing OSS and CPA that correspond to the real poles and zeros of R , we only need to calculate M_{11} and M_{21} . Using (11), (16), (17), (12), (15), (18), and doing the necessary algebra, we obtain

$$M_{11} = N_2, \quad M_{21} = -N_1, \quad (20)$$

where for both $\ell = 1, 2$,

$$N_\ell := P \left[n_\nu(k_2 a_2) \overleftrightarrow{\partial} h_\nu^{(\ell)}(ka_2) \right] + Q \left[j_\nu(k_2 a_2) \overleftrightarrow{\partial} h_\nu^{(\ell)}(ka_2) \right], \quad (21)$$

$$P := i(kk_2 a_1 a_2)^2 j_\nu(k_2 a_1) \overleftrightarrow{\partial} j_\nu(k_1 a_1), \quad Q := i(kk_2 a_1 a_2)^2 j_\nu(k_1 a_1) \overleftrightarrow{\partial} n_\nu(k_2 a_1). \quad (22)$$

In view of (20) – (22) and the fact that $f \overleftrightarrow{\partial} g = -g \overleftrightarrow{\partial} f$, we can express (19) in the form

$$R = - \frac{[j_\nu(k_2 a_1) \overleftrightarrow{\partial} j_\nu(k_1 a_1)] [n_\nu(k_2 a_2) \overleftrightarrow{\partial} h_\nu^{(2)}(ka_2)] - [n_\nu(k_2 a_1) \overleftrightarrow{\partial} j_\nu(k_1 a_1)] [j_\nu(k_2 a_2) \overleftrightarrow{\partial} h_\nu^{(2)}(ka_2)]}{[j_\nu(k_2 a_1) \overleftrightarrow{\partial} j_\nu(k_1 a_1)] [n_\nu(k_2 a_2) \overleftrightarrow{\partial} h_\nu^{(1)}(ka_2)] - [n_\nu(k_2 a_1) \overleftrightarrow{\partial} j_\nu(k_1 a_1)] [j_\nu(k_2 a_2) \overleftrightarrow{\partial} h_\nu^{(1)}(ka_2)]}.$$

Eqs. (20) provide a simple demonstration of the fact that CPA corresponds to an OSS of the time-reversed system. To see this we recall that we can obtain the time-reversed system by complex-conjugating the refractive indices \mathbf{n}_ℓ . This implies

$$k_\ell \rightarrow k_\ell^*, \quad P \rightarrow P^*, \quad Q \rightarrow Q^*, \quad N_1 \rightarrow N_2^*, \quad N_2 \rightarrow N_1^*, \quad (23)$$

$$M_{11} \rightarrow -M_{21}^*, \quad M_{21} \rightarrow -M_{11}^*, \quad R \rightarrow \frac{1}{R^*}, \quad (24)$$

where we have used (21), (22), (20), (19), and the fact that $h_\nu^{(1)}(ka_2)^* = h_\nu^{(2)}(ka_2)$. According to the last relation in (24), a CPA, that corresponds to $R = 0$, appears if and only if the reflection coefficient of the time-reversed system diverges, i.e., the latter develops an OSS and begins lasing at the threshold gain. Therefore, in the following we only consider the problem of locating OSS. We can easily obtain

the values of the physical parameters leading to a CPA of the spherical waves we consider by complex-conjugating the refractive indices \mathbf{n}_1 and \mathbf{n}_2 or changing the sign of the gain/attenuation coefficients of both the layers.

A straightforward consequence of this observation is the fact that because the law of energy conservation prohibits the emergence of an OSS for the case that both the interior core and the outer shell of our system consist of lossy material, a CPA cannot be realized unless either the core or the outer shell includes a lossy medium. Furthermore, it is possible to generate both a CPA and an OSS, if our system involves both lossy and gain media.

In order to determine the location of OSS in the space of the physical parameters of the system, we study the real zeros of M_{21} or alternatively N_1 in the complex k -plane. In view of (21) and (22), this is equivalent to finding the real values of k fulfilling

$$[j_\nu(k_2 a_1) \overleftrightarrow{\partial} j_\nu(k_1 a_1)] [n_\nu(k_2 a_1) \overleftrightarrow{\partial} h_\nu^{(1)}(k a_2)] = [n_\nu(k_2 a_1) \overleftrightarrow{\partial} j_\nu(k_1 a_1)] [j_\nu(k_2 a_1) \overleftrightarrow{\partial} h_\nu^{(1)}(k a_2)]. \quad (25)$$

Noting that $k_i = \mathbf{n}_i k$, this is a complex transcendental equation involving two complex variables, namely \mathbf{n}_1 and \mathbf{n}_2 , and two (positive) real variables: $x_1 := k a_1$ and $x_2 := k a_2$.

For $a_1 = a_2$ and $\mathbf{n}_1 = \mathbf{n}_2$ that corresponds to a homogeneous spherical medium that we consider in [11], the first factor on the left-hand side of (25) vanished identically and the first factor on its right-hand side becomes $W[n_\nu(x), j_\nu(x)]$ with $x = k_1 a_1 = x_1 \mathbf{n}_1$. Because the latter is nonzero, (25) reduces to

$$j_\nu(k_1 a_1) \overleftrightarrow{\partial} h_\nu^{(1)}(k a_1) = 0. \quad (26)$$

We can use the identity:

$$u'_\nu(z) = \frac{\nu u_{\nu-1}(z) - (\nu+1)u_{\nu+1}(z)}{2\nu+1}, \quad (27)$$

to express the derivative of the spherical Bessel, Neumann, and Hankel functions. Doing this in (26) gives rise to the equation for the spectral singularities of a spherical gain medium that we derive in [11], namely

$$\left. \frac{d}{dr} \ln h_\nu^{(1)}(kr) \right|_{r=a_1} = \left. \frac{d}{dr} \ln j_\nu(k_1 r) \right|_{r=a_1}. \quad (28)$$

Employing the identity (27) in (25) gives a more lengthy equation for OSS that we use in our numerical and graphical investigations. Before reporting the results of this investigation, however, we will carry out a perturbative analysis of (25). Similarly to the single-layer spherical medium we studied in [11], this turns out to reveal some basic properties of the solutions.

4 Perturbative Analysis of OSS

Consider the Mie regime where $a_2 \geq a_1 \gg 2\pi/k =: \lambda$ and $|\mathbf{n}_i| < 4$. Then $x_2 \geq x_1 \gg 1$, $|k_i a_1| = |\mathbf{n}_i| x_1 = 2\pi |\mathbf{n}_i| a_1 / \lambda \gg 1$, and we can perform a large- x_1 (and $-x_2$) expansion of the terms appearing in (25). This requires using the following asymptotic expansions of the spherical Bessel, Neumann, and Hankel functions.

$$j_\nu(z) = \frac{\sin(z - \frac{\pi\nu}{2})}{z} \sum_{s=0}^{\infty} \frac{(-1)^s \mathcal{A}_{2s}(\nu)}{z^{2s}} + \frac{\cos(z - \frac{\pi\nu}{2})}{z} \sum_{s=0}^{\infty} \frac{(-1)^s \mathcal{A}_{2s+1}(\nu)}{z^{2s+1}}, \quad (29)$$

$$n_\nu(z) = -\frac{\cos(z - \frac{\pi\nu}{2})}{z} \sum_{s=0}^{\infty} \frac{(-1)^s \mathcal{A}_{2s}(\nu)}{z^{2s}} + \frac{\sin(z - \frac{\pi\nu}{2})}{z} \sum_{s=0}^{\infty} \frac{(-1)^s \mathcal{A}_{2s+1}(\nu)}{z^{2s+1}}, \quad (30)$$

$$h_\nu^{(\ell)}(z) = \frac{e^{-i(-1)^\ell(z - \frac{\pi\nu}{2})}}{z} \left[i(-1)^\ell \sum_{s=0}^{\infty} \frac{(-1)^s \mathcal{A}_{2s}(\nu)}{z^{2s}} + \sum_{s=0}^{\infty} \frac{(-1)^s \mathcal{A}_{2s+1}(\nu)}{z^{2s+1}} \right], \quad (31)$$

where

$$\mathcal{A}_k(\nu) := \frac{\Gamma(\nu + k + 1)}{2^k k! \Gamma(\nu - k + 1)} = \frac{\prod_{\ell=0}^{2k-1} (\nu + k - \ell)}{2^k k!},$$

and Γ stands for the Gamma function.

Substituting (29) – (31) in (25), neglecting the quadratic and higher order terms in x_1^{-1} and x_2^{-1} in the resulting equation, noting that $\mathcal{A}_0(\nu) = 1$ and $\mathcal{A}_1(\nu) = \frac{\nu(\nu+1)}{2}$, and introducing

$$\mathbf{t}_\ell := \tan(k_\ell a_1 - \frac{\pi\nu}{2}) = \tan(x_1 \mathbf{n}_\ell - \frac{\pi\nu}{2}), \quad (32)$$

$$\mathcal{F}(x_1, \mathbf{n}_1, \mathbf{n}_2) := \frac{\mathbf{n}_1(\mathbf{n}_2 + i\mathbf{t}_2) + \mathbf{n}_2\mathbf{t}_1(\mathbf{n}_2\mathbf{t}_2 - i)}{\mathbf{n}_1(i - \mathbf{n}_2\mathbf{t}_2) + \mathbf{n}_2\mathbf{t}_1(\mathbf{n}_2 + i\mathbf{t}_2)}, \quad (33)$$

we find

$$\tan(x_2 \mathbf{n}_2 - \frac{\pi\nu}{2}) \approx \mathcal{F}(x_1, \mathbf{n}_1, \mathbf{n}_2), \quad (34)$$

where we use “ \approx ” to indicate that this equation is obtained by employing first-order perturbation theory. Solving (34) for x_2 yields

$$x_2 \approx \frac{\pi\nu + 2 \tan^{-1}(\mathcal{F})}{2 \mathbf{n}_2} = \frac{1}{2 \mathbf{n}_2} \left[\pi(2m + \nu) - i \ln \left(\frac{1 + i\mathcal{F}}{1 - i\mathcal{F}} \right) \right], \quad (35)$$

where we have used “ \ln ” to denote the principal part of natural logarithm of its argument, suppressed the argument of \mathcal{F} for brevity, and employed the identity

$$\tan^{-1}(z) = \pi m + \frac{1}{2i} \ln \left(\frac{1 + iz}{1 - iz} \right), \quad m = 0, \pm 1, \pm 2, \dots \quad (36)$$

The parameter m appearing in (35) is an integer that we identify with a mode number labeling OSS.

For a homogeneous spherical medium, where $a_1 = a_2$ and $\mathbf{n}_1 = \mathbf{n}_2$, we have $x_1 = x_2$, $\mathcal{F} = -i \mathbf{n}_1$, and (35) gives

$$x_1 \approx \frac{1}{2 \mathbf{n}_1} \left[\pi(2m + \nu + 1) - i \ln \left(\frac{\mathbf{n}_1 + 1}{\mathbf{n}_1 - 1} \right) \right]. \quad (37)$$

This is in complete agreement with Eq. (23) of Ref. [11].

Because the left-hand side of (35) is real, we can express this complex equation as a pair of real equations:

$$x_2 - \text{Re} \left\{ \frac{1}{2 \mathbf{n}_2} \left[\pi(2m + \nu) - i \ln \left(\frac{1 + i\mathcal{F}}{1 - i\mathcal{F}} \right) \right] \right\} \approx 0, \quad (38)$$

$$\text{Im} \left\{ \frac{1}{\mathbf{n}_2} \left[\pi(2m + \nu) - i \ln \left(\frac{1 + i\mathcal{F}}{1 - i\mathcal{F}} \right) \right] \right\} \approx 0. \quad (39)$$

We also note that

$$\frac{1 + i\mathcal{F}}{1 - i\mathcal{F}} = \frac{(\mathbf{n}_2\mathbf{t}_1 + i\mathbf{n}_1)(1 + i\mathbf{t}_2)(\mathbf{n}_2 + 1)}{(\mathbf{n}_2\mathbf{t}_1 - i\mathbf{n}_1)(1 - i\mathbf{t}_2)(\mathbf{n}_2 - 1)}. \quad (40)$$

Next, we consider the special case of a coated spherical active medium with $a_2 - a_1 \ll a_1$. In this case the gain/absorption properties of the coating can be neglected and \mathbf{n}_2 may be assumed to take a real value that we label by n_2 . This implies the equivalence of (39) and the condition that the absolute value of (40) must be unity. Imposing this condition and noting that in this case \mathbf{t}_2 is also real, we find

$$\left| \frac{n_2\mathbf{t}_1 + i\mathbf{n}_1}{n_2\mathbf{t}_1 - i\mathbf{n}_1} \right| \approx \frac{|n_2 - 1|}{n_2 + 1}. \quad (41)$$

This is a real equation involving a complex variable, \mathbf{n}_1 , and two real variables, n_2 and x_1 . In particular, it does not involve the mode number m .

In order to use (41) for locating OSS, we express \mathbf{n}_1 and \mathbf{t}_1 in terms of their real and imaginary parts. Let η_1 and κ_1 denote the real and imaginary parts of \mathbf{n}_1 , so that

$$\mathbf{n}_1 = \eta_1 + i\kappa_1, \quad (42)$$

and introduce

$$\alpha := x_1\eta_1 - \frac{\pi\nu}{2} = ka_1\eta_1 - \frac{\pi\nu}{2} = 2\pi \left(\frac{a_1\eta_1}{\lambda} - \frac{\nu}{4} \right), \quad \beta := x_1\kappa_1 = ka_1\kappa_1 = \frac{2\pi a_1\kappa_1}{\lambda}. \quad (43)$$

Then substituting (42) in (32) gives

$$\mathbf{t}_1 = \tan(\alpha + i\beta) = \frac{\tan \alpha + i \tanh \beta}{1 - i \tan \alpha \tanh \beta}. \quad (44)$$

Next, we use (42), (44), and various trigonometric and hyperbolic identities to obtain the following explicit form of (41).

$$\eta_1 \sinh(2\beta) - \kappa_1 \sin(2\alpha) + \left(\frac{\eta_1^2 + \kappa_1^2 + n_2^2}{n_2^2 + 1} \right) \cosh(2\beta) + \left(\frac{\eta_1^2 + \kappa_1^2 - n_2^2}{n_2^2 + 1} \right) \cos(2\alpha) \approx 0. \quad (45)$$

A similar analysis reveals the fact that the following quantity is an integer.

$$\tilde{m} := \gamma - \pi^{-1} \arg \left(\frac{1 + i\mathcal{F}}{1 - i\mathcal{F}} \right), \quad (46)$$

where

$$\gamma := \frac{4a_1n_2}{\lambda} + \xi - \nu, \quad (47)$$

$$\xi := \pi^{-1} \arctan \left\{ \frac{2n_2[\eta_1 \sin(2\alpha) + \kappa_1 \sinh(2\beta)]}{[n_2^2 - (\eta_1^2 + \kappa_1^2)] \cosh(2\beta) - [n_2^2 + \eta_1^2 + \kappa_1^2] \cos(2\alpha)} \right\}, \quad (48)$$

and “ $\arg(z)$ ” denotes the principal argument of z that takes values in $(-\pi, \pi]$. The latter implies that \tilde{m} is one of the two integers satisfying the condition:

$$\gamma - 1 \leq \tilde{m} < \gamma + 1. \quad (49)$$

A more important implication of (46) is that it leads to the following explicit form of (38).

$$a_2 - a_1 \approx a_0 + \frac{\lambda(2m - \tilde{m})}{4n_2}, \quad (50)$$

where

$$a_0 := \frac{\lambda\xi}{4n_2}. \quad (51)$$

Note that the “ \arctan ” appearing in (48) stands for the principal value of “ \tan^{-1} ” that takes values in $[-\frac{\pi}{2}, \frac{\pi}{2}]$. This in particular implies that $|\xi| \leq 1/2$. Therefore,

$$|a_0| \leq \frac{\lambda}{8n_2}. \quad (52)$$

Another useful relation that follows from (47), (48), and (51) is

$$\gamma = \frac{4n_2(a_1 + a_0)}{\lambda} - \nu. \quad (53)$$

Eq. (50) is quite remarkable, for it indicates that if we choose η_1, κ_1, n_2 and $x_1 = 2\pi a_1/\lambda$ so that $x_1 \gg 1$ and (45) holds, then an OSS arises for a discrete set of values of the thickness of the coating. Because $2m - \tilde{m}$ is an integer, according to (50) and (52),

$$2m \gtrsim \tilde{m} \geq \gamma - 1, \quad a_2 - a_1 \gtrsim \frac{\lambda}{8n_2}. \quad (54)$$

This means that the mode number m and the thickness $a_2 - a_1$ are bounded from below by $(\gamma - 1)/2$ and $\lambda/(8n_2)$, respectively. Notice that these bounds only depend on a_1, λ and n_2 .

Next, we examine the physical implications of (45) for a typical optically active material that satisfies

$$|\kappa_1| \ll |\beta| \ll \eta_1 \ll \alpha. \quad (55)$$

In this case, we can ignore the terms of order two and higher in κ_1 and β in our calculations. Implementing this approximation in (45), using (43), and recalling that the imaginary part of \mathbf{n}_1 , i.e., κ_1 , is related to the gain coefficient g via $\kappa_1 = -g\lambda/(4\pi)$, we find

$$a_1 g \approx \frac{\eta_1^2 + n_2^2 + (\eta_1^2 - n_2^2) \cos(2\alpha)}{\eta_1(n_2^2 + 1)}. \quad (56)$$

This relation shows that the radius a_1 of the inner core is inversely proportional to the gain coefficient. Furthermore, it puts curious upper and lower bounds on the possible values of a_1 that are only sensitive to the gain coefficient and the real part of the refractive indices of the inner core and the outer shell:

$$\frac{2n_{\min}^2}{\eta_1 g(n_2^2 + 1)} \lesssim a_1 \lesssim \frac{2n_{\max}^2}{\eta_1 g(n_2^2 + 1)}, \quad (57)$$

where n_{\max} and n_{\min} are respectively the largest and smallest of η_1 and n_2 .

In view of (57), the larger n_2 is, the smaller the lower bound of a_1 gets. This confirms our expectation that coating a spherical gain medium by a material with higher refractive index reduces the lower bound on the radius of the gain medium. For example, if we take $n_2 = 2.5$ and choose the inner core to be made of a dye gain material with $\eta_1 \approx 1.48$ and $g \approx 5 \text{ cm}^{-1}$, we find

$$0.816 \text{ mm} \lesssim a_1 \lesssim 2.330 \text{ mm}. \quad (58)$$

Finally, we explore the consequences of (55). Implementing the above approximation scheme of neglecting second and higher order terms in β and κ_1 in (50) yields

$$a_0 \approx \frac{\lambda}{4\pi n_2} \arctan \left\{ \frac{2\eta_1 n_2 \sin(2\alpha)}{n_2^2 - \eta_1^2 - (\eta_1^2 + n_2^2) \cos(2\alpha)} \right\}. \quad (59)$$

Taking $a_1 = 1 \text{ mm}$ to comply with (58), choosing $\lambda = 549 \text{ nm}$, $\eta_1 \approx 1.48$, and $n_2 = 2.5$ as above, and using (50), (47), (49), (54) and (59) we find

$$a_2 - a_1 \approx [55(2m - \tilde{m}) + 27] \text{ nm}, \quad \tilde{m} \approx \gamma = 18122. \quad (60)$$

The smallest allowed value of the thickness is therefore $a_2 - a_1 \approx a_0 = 27 \text{ nm}$.

In practice the thickness of the coating has a fixed value, and (59) and (60) determine an approximate value of the mode number m :

$$m \approx \frac{2n_2(a_2 - a_1 - a_0)}{\lambda} + \frac{\tilde{m}}{2}. \quad (61)$$

If we further approximate \tilde{m} by γ and use the expression (53) for the latter, then (61) gives

$$m \approx \frac{2n_2 a_2}{\lambda} - \frac{\nu}{2}. \quad (62)$$

For example, for $a_2 - a_1 = 5 \mu\text{m}$, this relation gives $m \approx 9152$, which coincides with the numerical result obtained directly from (38).

We can also use (62) to express the wavelength of the OSS in terms of the mode number. This gives

$$\lambda \approx \frac{4n_2a_2}{2m + \nu}. \quad (63)$$

The analogous expression for the case that we remove the coating is given by Eq. (33) of Ref. [11] and reads

$$\lambda \approx \frac{4\eta_1a_1}{2m + \nu + 1} \approx \frac{4\eta_1a_1}{2m + \nu}. \quad (64)$$

Comparing (63) with (64) and noting that $n_2a_2 > \eta_1a_1$, we can see that the presence of the coating increases the wavelength of the OSS associated for each mode number. Alternatively, it increases the value of the mode number for an OSS of given wavelength.

We conclude this section by pointing out that we can perform a perturbative calculation of OSS in a way that avoids the explicit appearance of the mode number m . According to (50) and (51), $\tan[4\pi n_2(a_2 - a_1)/\lambda] = \tan(\pi\xi)$. In light of (48) we can easily compute $\tan(\pi\xi)$ and express the latter equation in the form

$$\begin{aligned} & \{(n_2^2 + \eta_1 + \kappa_1) \cos(2\alpha) - (n_2^2 - \eta_1 - \kappa_1) \cosh(2\beta)\} \sin[4\pi n_2 \lambda^{-1}(a_2 - a_1)] \\ & + 2n_2 \{\eta_1 \sin(2\alpha) + \kappa_1 \sinh(2\beta)\} \cos[4\pi n_2 \lambda^{-1}(a_2 - a_1)] = 0. \end{aligned} \quad (65)$$

In summary, we have obtained the real equations (45) and (65) by imposing the complex equation (34). We derived the latter by performing first-order perturbation theory on (25) that determined OSS. It is important to note that every solution of (34) is a solution of (45) and (65), but the converse may not be true. We have checked for some concrete examples and found that indeed this is the case. Therefore, we solve (45) and (65) by fixing all but two of the real parameters entering in these equations and then eliminate the solutions that violate (34).

5 OSS of a Concrete Two-Layer Spherical Medium

In general the refractive index \mathbf{n} of an optically active medium depends on the properties of the medium and the wavelength of the propagating EM wave. For example, for a gain medium that is obtained by doping a host medium of refraction index n_0 and modeled by a two-level atomic system with lower and upper level population densities N_l and N_u , resonance frequency ω_0 , and damping coefficient γ , it satisfies the dispersion relation [8]:

$$\mathbf{n}^2 = n_0^2 - \frac{\hat{\omega}_p^2}{\hat{\omega}^2 - 1 + i\hat{\gamma}\hat{\omega}}, \quad (66)$$

where $\hat{\omega} := \omega/\omega_0$, $\hat{\gamma} := \gamma/\omega_0$, $\hat{\omega}_p := (N_l - N_u)e^2/(m_e\epsilon_0\omega_0^2)$, e is electron's charge, and m_e is its mass. We can express $\hat{\omega}_p^2$ in terms of the imaginary part κ_0 of \mathbf{n} at the resonance wavelength $\lambda_0 := 2\pi c/\omega_0$ according to [8]

$$\hat{\omega}_p^2 \approx 2n_0\hat{\gamma}\kappa_0, \quad (67)$$

where the approximation symbol means that we neglect quadratic and higher order terms in κ_0 .

Inserting (67) in (66) and using $\mathbf{n} = \eta + i\kappa$, we obtain

$$\eta \approx n_0 + \kappa_0 f_1(\hat{\omega}), \quad \kappa \approx \kappa_0 f_2(\hat{\omega}), \quad (68)$$

where

$$f_1(\hat{\omega}) := \frac{\hat{\gamma}(1 - \hat{\omega}^2)}{(1 - \hat{\omega}^2)^2 + \hat{\gamma}^2 \hat{\omega}^2}, \quad f_2(\hat{\omega}) := \frac{\hat{\gamma}^2 \hat{\omega}}{(1 - \hat{\omega}^2)^2 + \hat{\gamma}^2 \hat{\omega}^2}. \quad (69)$$

We also note that the gain coefficient of such a medium is given by $g = -4\pi\kappa/\lambda$. In particular, we can use this relation to express κ_0 in terms of the gain coefficient g_0 at the resonance wavelength λ_0 according to

$$\kappa_0 = -\frac{\lambda_0 g_0}{4\pi}. \quad (70)$$

In the following, we employ (68) – (70) to parameterize the refractive indices \mathbf{n}_1 and \mathbf{n}_2 that enter in the description of our two-layer spherical model.

In order to explore the effect of the outer shell on the behavior of spectral singularities, we consider a spherical dye laser medium confined in a thin spherical shell of higher-refractive index glass. We suppose that the refractive index of the glass takes a constant real value and parameterize the location of the spectral singularities using the resonance gain coefficient, g_0 , of the dye and the wavelength λ .

Consider confining a Rose Bengal-DMSO (Dimethyl sulfoxide) solution with characteristics [18, 19]

$$n_0 = 1.479, \quad \lambda_0 = 549 \text{ nm}, \quad \hat{\gamma} = 0.062, \quad g_0 \leq 5 \text{ cm}^{-1}, \quad (71)$$

in a spherical glass shell of outer radius $a_2 = 1$ mm, thickness $a_2 - a_1 = 5 \mu\text{m}$, and refractive index $n_2 = 2.5$.³ Figure 2 and Table 1 show the results of our numerical calculation of the location of spectral singularities that use (25). Table 1 also gives the results of our perturbative calculations and

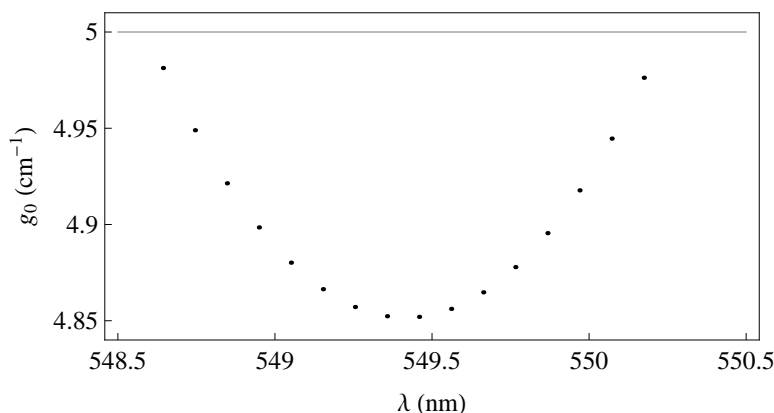


Figure 2: Spectral singularities of the Rose Bengal-DMSO dye gain medium (71) confined in a spherical glass shell of outer radius 1 mm, thickness $5 \mu\text{m}$, and refractive index 2.5. The minimum corresponds to $\lambda = \lambda^{(1)} \approx 549.459$ nm that is larger than the resonance wavelength $\lambda_0 = 549$ nm. The grey horizontal line represents the experimental upper bound on g_0 .

demonstrates their good agreement with the numerical results.

Let $g_0^{(1)}$ denote the smallest value of the gain coefficient g_0 that is capable of producing an OSS, and $\lambda^{(1)}$ be the wavelength of this OSS. We recall from Ref. [11] that in the absence of coating $\lambda^{(1)}$ is essentially identical with the resonance wavelength λ_0 . According to Figure 2 and Table 1, the presence of the glass coating causes $\lambda^{(1)}$ to be slightly red-shifted.

Figure 3 shows a logarithmic plot of the reflection coefficient as a function of the wavelength for the sample considered in Figure 2 and Table 1 with $g_0 = g_0^{(3)} = 4.85614735 \text{ cm}^{-1}$. In this case, there is an OSS at $\lambda = \lambda^{(3)} = 549.56092702$ nm that corresponds to the central peak in Figure 3. Unlike

³For the details of developing such a high-refractive index glass, see [20, 21].

ℓ	m	$g_0^{(\ell)}$ (cm ⁻¹)	$\lambda_{\text{pert.}}^{(\ell)}$ (nm)	$\lambda_{\text{exact}}^{(\ell)}$ (nm)
1	9099	4.8520	549.458833	549.458836
2	9101	4.8523	549.356779	549.356781
3	9098	4.8561	549.560925	549.560927
4	9103	4.8571	549.254762	549.254765
5	9096	4.8647	549.663054	549.663056
6	9104	4.8664	549.152785	549.152787
7	9094	4.8779	549.765220	549.765222

Table 1: The mode number m , gain coefficient g_0 , and wavelength $\lambda^{(\ell)}$ for the spectral singularities of the Rose Bengal-DMSO dye gain medium (71) confined in a spherical glass shell of outer radius 1 mm, thickness 5 μm , and refractive index 2.5. The subscripts “exact” and “pert.” refer to the results of numerical and perturbative calculations, respectively. These calculations give the same values for g_0 up to six significant figures.

the other peaks shown in this figure, the height of the central peak increases indefinitely as we use more and more accurate numerical values for the parameters of the system. This is a clear indication that it corresponds to a spectral singularity.

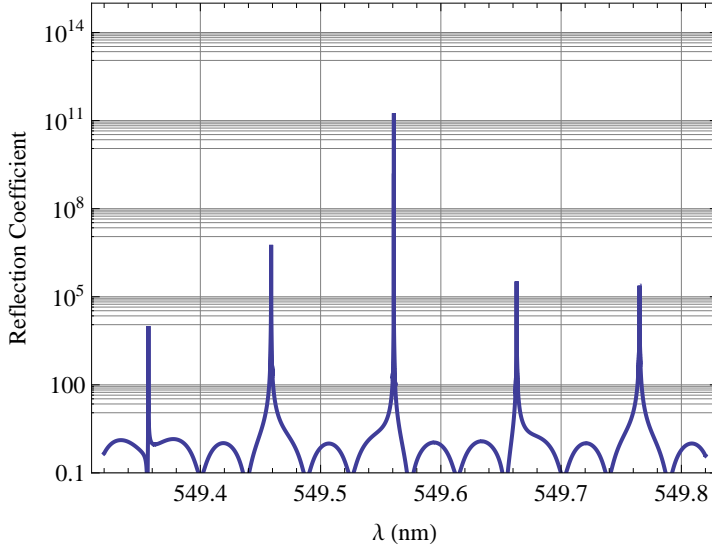


Figure 3: (Color online) Graph of reflection coefficient for the outer radius of 1 mm and thickness of 5 μm when the gain coefficient is $g_0^{(3)} = 4.85614735 \text{ cm}^{-1}$. The central peak represents an OSS.

Next, we explore the effect of changing the thickness of coating $a_2 - a_1$ on the $\lambda^{(1)}$ while keeping the inner radius fixed. Figure 4 shows the graph of $\lambda^{(1)}$ as a function of thickness. As seen from this figure, as we increase the thickness, $\lambda^{(1)}$ undergoes an infinite set of jumps that oscillate about the resonance wavelength λ_0 with a decreasing amplitude. Our numerical results show that unlike the wavelength $\lambda^{(1)}$, the gain coefficient $g_0^{(1)}$ does not experience a noticeable change due to an increase in the thickness.

Figure 5 shows the location of OSS for a spherical dye gain medium without a coating. Comparing this figure with Figure 2, we see that except for the shift in the value of $\lambda^{(1)}$, the distribution of the OSS in the g_0 - λ plane does not seem to get affected by the presence of the coating glass. Exploring a wider range of values of λ and g_0 reveals a different picture. Figures 6 and 7 show the location of OSS

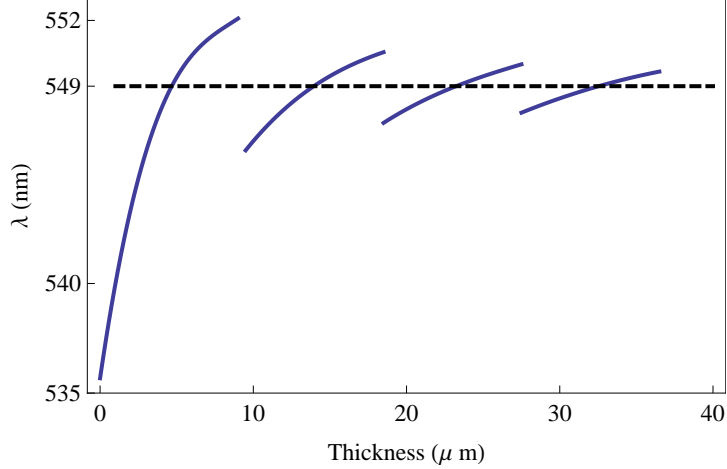


Figure 4: (Color online) Graph of the wavelength $\lambda^{(1)}$ as a function of the thickness of coating. The inner radius is held at $a_1 = 1.6$ mm. As we change the thickness, $\lambda^{(1)}$ undergoes an infinite set of jumps that oscillate about λ_0 with a decreasing amplitude.

in a wider spectral range for a coated spherical Rose Bengal-DMSO sample with specifics (71), inner radius 1.5 mm, and two different values of the coating thickness, namely $5 \mu\text{m}$ and $10 \mu\text{m}$. As these figures show, OSS are located on curves with multiple local minima. The number of these minima that fulfill the experimental upper bound of $g_0 \leq 5 \text{ cm}^{-1}$ is an increasing function of the thickness of the coating. For $a_2 - a_1 = 5 \mu\text{m}$ (Figure 6), this number is three, i.e., there are three distinct groups of OSS satisfying the bound: $g_0 \leq 5 \text{ cm}^{-1}$. These appear in the spectral ranges 536.941436-539.544783 nm, 546.335226-552.571190 nm, and 560.400334-561.815048 nm and respectively contain 41, 93, and 21 members. Their central member that corresponds to the smallest gain coefficient appear at $(\lambda, g_0) = (538.239847, 4.601744)$, $(549.435560, 3.218290)$, and $(561.106835, 4.895167)$ in $(\text{nm}, \text{cm}^{-1})$ units. For $a_2 - a_1 = 10 \mu\text{m}$ (Figure 7), there are four groups of OSS satisfying the bound on g_0 . They include 34, 47, 46, and 30 members with wavelengths ranging over 539.621948-541.782279 nm, 544.992898-548.067753 nm, 550.878022-553.951299 nm, and 557.516880-559.542755 nm, respectively. The central members of these four groups that correspond to the local minima of g_0 have (λ, g_0) values: $(540.666848, 4.010267)$, $(546.525852, 3.287748)$, $(552.444850, 3.348007)$ and $(558.493430, 4.217539)$ in $(\text{nm}, \text{cm}^{-1})$ units. In particular, the presence of the glass coating not only allows for generating OSS in a smaller gain medium, but it produces spectral gaps in the spectral range within which these OSS are located. These remarkable observations should in principle be verifiable experimentally.

Next, we study the effect of changing the radius of the inner core on the location of OSS for a fixed value of the coating thickness. Figure 8 shows the graph of the minimum gain coefficient g_0 necessary for generating an OSS as a function of a_1 for the coated spherical Rose Bengal-DMSO dye gain medium with specifications (71) and thickness $5 \mu\text{m}$. For $a_1 \leq a_1^{(\text{min})} \approx 0.96$ mm no OSS can be created. Recalling that for an uncoated sample $a_1^{(\text{min})} \approx 3.3$ mm, this corresponds to a three-fold decrease in the size of the gain medium. As we increase a_1 starting from the critical value 0.96 mm, the minimum gain coefficient necessary for generating an OSS, namely $g_0^{(1)}$ decreases. Both of these observations are in agreement with our perturbative results. Moreover, it turns out that for fixed values of the coating thickness the wavelength $\lambda^{(1)}$ is not sensitive to the variations of the inner radius. Figure 9 demonstrates this behavior. As our perturbative treatment shows the larger the refractive index of coating is the smaller the minimum radius $a_1^{(\text{min})}$ gets. For example if we use a glass coating with the same thickness ($5 \mu\text{m}$) but a slightly lower index of refraction, say $n_2 = 1.93$ as in [20], the value of $a_1^{(\text{min})}$ increases by

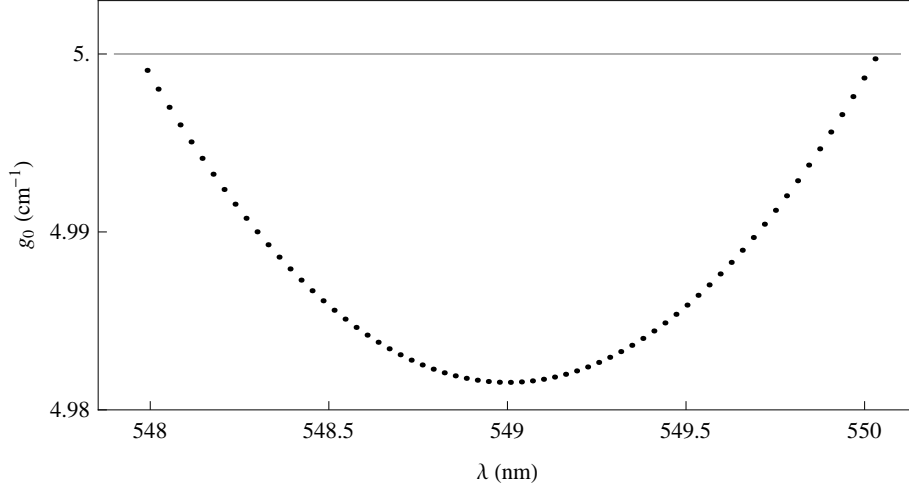


Figure 5: OSS of an uncoated spherical Rose Bengal-DMSO dye gain medium with specifications (71) and radius 3.3 mm. The minimum gain coefficient necessary for generating an OSS and the corresponding wavelength are respectively 4.9815 cm^{-1} and 549.008 nm . The horizontal grey line represents the experimental upper bound on g_0 . There are 66 OSS complying with this bound.

a factor of 2 (to about 1.8 mm.)

We have also investigated the formation of OSS in a two-layer spherical model in which the inner core is made of a higher-refractive index glass and the outer shell is filled with a dye gain material. Using the same glass and gain material and taking the core radius to be 2 mm, we found that the minimum shell thickness required for producing an OSS was about 3.28 mm. This coincides with the minimum radius supporting an OSS for a sphere filled with the same gain material. Figure 10 shows the location of OSS for the thickness of 3.3 mm as given by (25). The main difference between this figure and Figure 5 is that the number of OSS has doubled. To our knowledge this is the only effect of the presence of the glass core. We also find that using a glass core with a lower index of refraction does not have a sizable effect on the location and number of OSS.

6 Concluding Remarks

A gain medium can emit electromagnetic waves provided that we adjust its parameters so that an optical spectral singularity is created. The time-reversal of this phenomenon corresponds to the (coherent perfect) absorption of electromagnetic waves. This is the theoretical basis of antilasing. The simplest example of a gain medium that is localized in space and is capable of realizing an optical spectral singularity is a spherical gain medium. It supports spectral singularities in a radial transverse mode provided that its radius exceeds a critical value $a^{(\min)}$.

For the typical dye laser material that we consider in Ref. [11], $a^{(\min)} \approx 3.28 \text{ mm}$. In practice maintaining a uniform gain coefficient within a spherical sample of this size can be difficult. The main motivation for the current study is the idea that coating a spherical gain medium by a high-refractive index material can reduce $a^{(\min)}$. We have shown by explicit perturbative and numerical calculations that this is actually the case. In particular, coating a spherical active dye medium with a glass of thickness $5 \mu\text{m}$ and index of refractive 2.5 reduces $a^{(\min)}$ by about a factor of 3. Furthermore, we have found that the presence of coating leads to a much richer structure as far as the location of spectral singularities are concerned. In particular, the coating causes a small shift in the wavelength of the

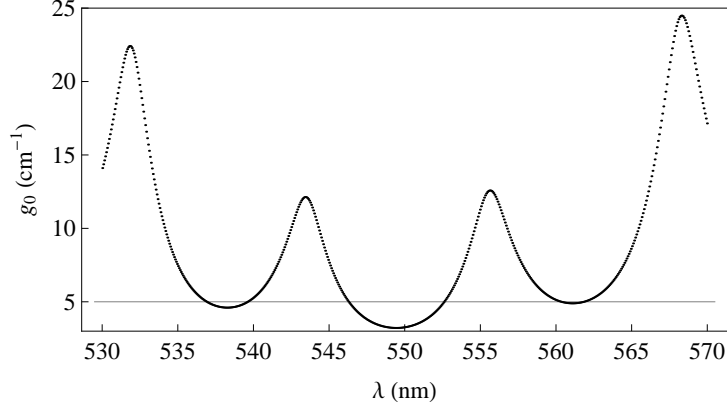


Figure 6: OSS of a coated spherical Rose Bengal-DMSO dye gain medium with specifications (71), inner radius 1.5 mm, and coating thickness $5 \mu\text{m}$. The horizontal grey line represents the experimental upper bound on g_0 . There are three groups of OSS below this bound. They appear in the spectral ranges 536.941436-539.544783 nm, 546.335226-552.571190 nm, and 560.400334-561.815048 nm and contain 41, 93, and 21 members, respectively.

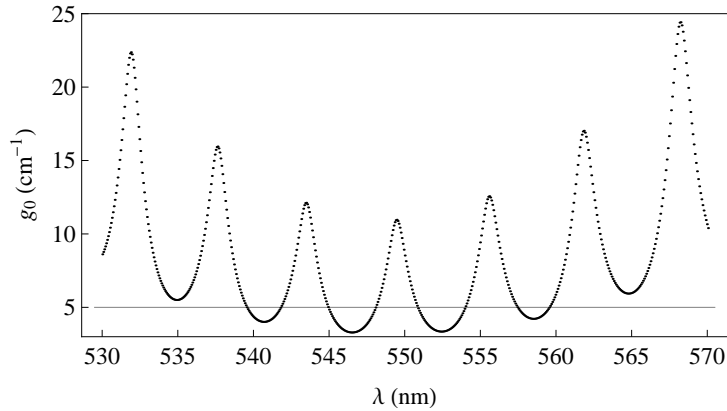


Figure 7: OSS of a coated spherical Rose Bengal-DMSO dye gain medium with specifications (71), inner radius 1.5 mm, and coating thickness $10 \mu\text{m}$. There are four groups of OSS fulfilling the experimental upper bound on g_0 (the horizontal grey line.) They appear in the spectral ranges 539.621948-541.782279 nm, 544.992898-548.067753 nm, 550.878022-553.951299 nm, and 557.516880-559.542755 nm and contain 34, 47, 46, and 30 members, respectively.

spectral singularity that requires the least amount of gain. More importantly, it produces a clustering of spectral singularities into groups separated by sizable spectral gaps. This behavior may find an application in producing tunable lasers with rather wide spectral gaps. Another interesting possibility is to generate laser pulses in different spectral ranges by periodically altering the gain coefficients of the active core. For example, as shown in Figures 6 and 8, increasing the gain coefficient so that it passes one or more of the local minima of the OSS curves leads to lasing in two or more spectral ranges that are separated by gaps of several nm in width.⁴

If we use a glass spherical core and an active dye outer shell, the thickness of the shell required

⁴For an experimental realization of the OSSs we have examined and their possible applications, one may try to use the SHG of a diode pumped Nd-YAG (continuous wave) laser at 532 nm wavelength in the plane-wave configuration. To achieve reasonably uniform gain, one probably needs to use multiple pumping. The details and a discussion of alternative pumping methods are beyond the scope of the present paper and the expertise of the authors.

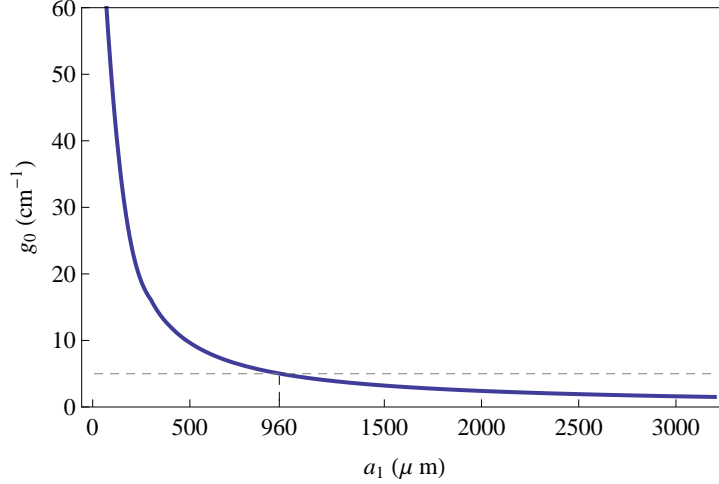


Figure 8: (Color online) Graph of g_0 as a function of the inner radius a_1 . The coating thickness is kept fixed at $5 \mu\text{m}$. Dashed line corresponds to the experimental bound $g_0 \leq 5\text{cm}^{-1}$. For $g_0 = 5 \text{cm}^{-1}$ the smallest value of the inner radius that supports an OSS is about $960 \mu\text{m}$. For larger values of a_1 , there are OSS with $g_0 < 5 \text{cm}^{-1}$.

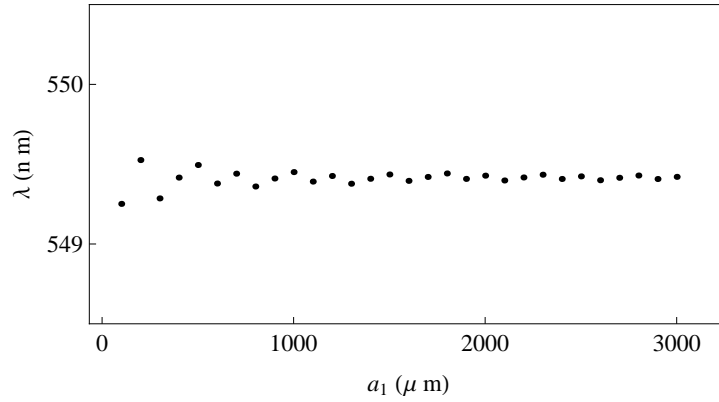


Figure 9: Effect of changing the inner radius on the wavelength $\lambda^{(1)}$ for the coating thickness of $5 \mu\text{m}$. The displayed dots correspond to increments of the radius a_1 of $100 \mu\text{m}$. For continuous variations of the radius these dots fluctuate around the line $\lambda^{(1)} = 549.4 \text{ nm}$ with a decreasing amplitude as the gain coefficient increases.

to induce an optical spectral singularity is about the $a^{(\text{min})}$ for an uncoated spherical gain medium consisting of the same dye. The presence of the glass core does not seem to have a significant effect except for the doubling of the number of the spectral singularities. We plan to explore the reasons for this phenomenon in a more general context.

The results we have reported apply for a TEM electromagnetic wave propagating in the radial direction. As we show in the appendix, we can extend our investigation to study optical spectral singularities for electromagnetic waves in the TE and TM modes. It turns out that the results are similar to those for the TEM mode. For example the size of the a^{min} remains essentially the same.

The emergence of an optical spectral singularity is a common feature of any lasing system. This includes typical coated or uncoated spherical lasers that can be realized using much smaller, micron size dye samples [20, 22]. The reason is that these lasers involve exciting whispering gallery modes [15]. We intend to conduct a through study of optical spectral singularities for whispering gallery modes.

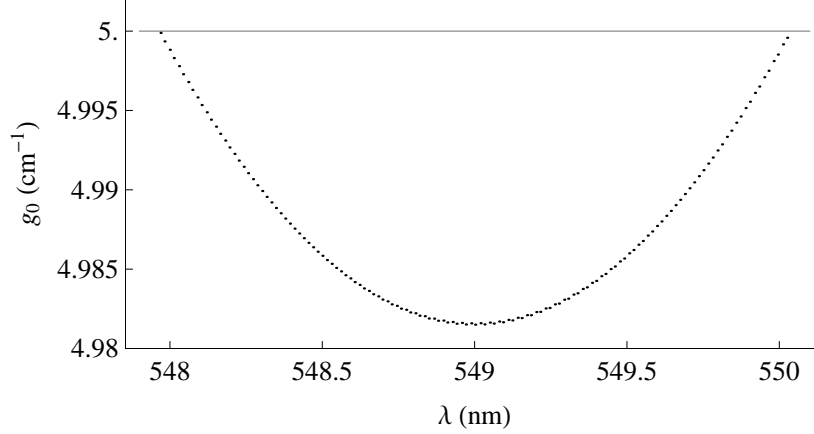


Figure 10: OSS for a double-layer sphere consisting of a glass core with refractive index $n_1 = 2.5$ and an outer shell filled with a Rose Bengal-DMSO dye solution with specifics (71). The inner and outer radii are taken as $a_1 = 2$ nm and $a_2 = 5.3$ nm. The grey line represents the experimental upper bound on g_0 . There are 136 OSS fulfilling this bound. They are located in the spectral range: 547.969294-550.025813 nm. The OSS with minimum gain has coordinates $\lambda^{(1)} = 549.001882$ nm and $g_0^{(1)} = 4.981501$ cm^{-1} .

Acknowledgments: We wish to express our gratitude to Ali Serpengüzel for reading the draft of this article and making many useful comments and suggestions. This work has been supported by the Scientific and Technological Research Council of Turkey (TÜBİTAK) in the framework of the project no: 110T611 and the Turkish Academy of Sciences (TÜBA).

Appendix

In this appendix we extend our analysis of optical spectral singularities to the general TE(ℓ, m) and TM(ℓ, m) modes of our two-layer spherical system.

We begin our treatment by writing the solutions of the Maxwell's equations in TE and TM modes of a spherical system as follows [17].

$$\vec{E} = Z_0 \sum_{\ell, m} \left[\frac{i}{k_3(r)} a_M(\ell, m) \vec{\nabla} \times f_\ell(\tilde{k}r) \vec{X}_{\ell m} + a_E(\ell, m) g_\ell(\tilde{k}r) \vec{X}_{\ell m} \right] \quad (72)$$

$$\vec{H} = \sum_{\ell, m} \left[a_M(\ell, m) f_\ell(\tilde{k}r) \vec{X}_{\ell m} - \frac{i}{k} a_E(\ell, m) \vec{\nabla} \times g_\ell(\tilde{k}r) \vec{X}_{\ell m} \right] \quad (73)$$

where ℓ and m take integer values in ranges $[0, \infty)$ and $[-\ell, \ell]$ respectively, a_E and a_M are the coefficients of TE and TM modes respectively, $Z_0 := \sqrt{\mu_0/\epsilon_0}$ is the impedance of the vacuum, $\mathfrak{z}(r)$ is given in (3), both $f_\ell(\tilde{k}r)$ and $g_\ell(\tilde{k}r)$ have form

$$f_\ell(\tilde{k}r), g_\ell(\tilde{k}r) = \begin{cases} A_1 j_\nu(k_1 r) + B_1 n_\nu(k_1 r) & \text{for } r < a_1, \\ A_2 j_\nu(k_2 r) + B_2 n_\nu(k_2 r) & \text{for } a_1 < r < a_2, \\ A_3 h_\nu^{(1)}(k r) + B_3 h_\nu^{(2)}(k r) & \text{for } r > a_2, \end{cases} \quad (74)$$

$\vec{X}_{\ell m}(\theta, \phi) := \frac{1}{\sqrt{\ell(\ell+1)}} \vec{L} Y_{\ell, m}$, $\vec{L} := -i\vec{r} \times \vec{\nabla}$, $Y_{\ell, m}$ are spherical harmonics:

$$Y_{\ell, m}(\theta, \phi) := \sqrt{\frac{2\ell+1}{4\pi} \frac{(\ell-m)!}{(\ell+m)!}} P_\ell^m(\cos \theta) e^{im\phi},$$

and P_ℓ^m are the associated Legendre functions. Note that $\vec{X}_{\ell m}$ fulfil the orthogonality relations: $\int \vec{X}_{\ell' m'}^* \cdot \vec{X}_{\ell m} d\Omega = \delta_{\ell\ell'} \delta_{mm'}$ and $\int \vec{X}_{\ell' m'}^* \cdot (\vec{r} \times \vec{X}_{\ell m}) d\Omega = 0$, where $d\Omega := \sin\theta d\theta d\phi$, and being proportion to the angular momentum operator, \vec{L} satisfies $L^2 Y_{\ell m} = \ell(\ell+1) Y_{\ell m}$.

Expressing the electric and magnetic fields in terms of their components in the spherical coordinates, we have $\vec{E} = \hat{r}E_r(r, \theta, \phi) + \hat{\theta}E_\theta(r, \theta, \phi) + \hat{\phi}E_\phi(r, \theta, \phi)$ and $\vec{H} = \hat{r}H_r(r, \theta, \phi) + \hat{\theta}H_\theta(r, \theta, \phi) + \hat{\phi}H_\phi(r, \theta, \phi)$, where

$$\begin{aligned}
E_r &= Z_0 \sum_{\ell, m} \frac{a_E(\ell, m) b(\ell, m) f_\ell(\tilde{k}r)}{kr\mathfrak{z}(r)} \left[\frac{\partial \Pi_{\ell, m}(\theta)}{\partial \theta} - m^2 \frac{\Omega_{\ell, m}(\theta)}{\sin \theta} \right] e^{im\phi} \\
E_\theta &= -Z_0 \sum_{\ell, m} b(\ell, m) \left[\frac{a_E(\ell, m)}{k\mathfrak{z}(r)} \frac{\partial f_\ell(\tilde{k}r)}{\partial r} \Pi_{\ell, m}(\theta) + ma_M(\ell, m) g_\ell(\tilde{k}r) \Omega_{\ell, m}(\theta) \right] e^{im\phi} \\
E_\phi &= -iZ_0 \sum_{\ell, m} b(\ell, m) \left[\frac{ma_E(\ell, m)}{k\mathfrak{z}(r)} \frac{\partial f_\ell(\tilde{k}r)}{\partial r} \Omega_{\ell, m}(\theta) + a_M(\ell, m) g_\ell(\tilde{k}r) \Pi_{\ell, m}(\theta) \right] e^{im\phi} \\
H_r &= - \sum_{\ell, m} \frac{a_M(\ell, m) b(\ell, m) g_\ell(\tilde{k}r)}{kr} \left[\frac{\partial \Pi_{\ell, m}(\theta)}{\partial \theta} - m^2 \frac{\Omega_{\ell, m}(\theta)}{\sin \theta} \right] e^{im\phi} \\
H_\theta &= \sum_{\ell, m} b(\ell, m) \left[-ma_E(\ell, m) f_\ell(\tilde{k}r) \Omega_{\ell, m}(\theta) + \frac{a_M(\ell, m)}{k} \frac{\partial g_\ell(\tilde{k}r)}{\partial r} \Pi_{\ell, m}(\theta) \right] e^{im\phi} \\
H_\phi &= i \sum_{\ell, m} b(\ell, m) \left[-a_E(\ell, m) f_\ell(\tilde{k}r) \Pi_{\ell, m}(\theta) + \frac{ma_M(\ell, m)}{k} \frac{\partial g_\ell(\tilde{k}r)}{\partial r} \Omega_{\ell, m}(\theta) \right] e^{im\phi} \\
b(\ell, m) &:= \frac{1}{\ell(\ell+1)} \sqrt{\frac{2\ell+1}{4\pi} \frac{(\ell-m)!}{(\ell+m)!}}, \quad \Pi_{\ell, m}(\theta) := \frac{\partial}{\partial \theta} P_\ell^m(\cos \theta), \quad \Omega_{\ell, m}(\theta) := \frac{P_\ell^m(\cos \theta)}{\sin \theta}.
\end{aligned}$$

Imposing the physical matching conditions at $r = a_1$ and $r = a_2$, we find that the tangential components of \vec{E} and \vec{H} are continuous along the boundaries, i.e., $E_\theta^{in} = E_\theta^{out}$, $E_\phi^{in} = E_\phi^{out}$, $H_\theta^{in} = H_\theta^{out}$, and $H_\phi^{in} = H_\phi^{out}$.

For TE modes, we can express these boundary conditions as

$$\mathbf{K}_{11}^E \begin{bmatrix} a_{E1} \\ 0 \end{bmatrix} = \mathbf{K}_{12}^E \begin{bmatrix} a_{E2} \\ b_{E2} \end{bmatrix}, \quad \mathbf{K}_{22}^E \begin{bmatrix} a_{E2} \\ b_{E2} \end{bmatrix} = \mathbf{L}^E \begin{bmatrix} a_{E3} \\ b_{E3} \end{bmatrix}, \quad (75)$$

where for all $p, q = 1, 2$,

$$\mathbf{K}_{pq}^E := \begin{bmatrix} j_\ell(k_q a_p) & n_\ell(k_q a_p) \\ \tilde{j}_\ell(k_q a_p) & \tilde{n}_\ell(k_q a_p) \end{bmatrix}, \quad \mathbf{L}^E := \begin{bmatrix} h_\ell^{(1)}(ka_2) & h_\ell^{(2)}(ka_2) \\ \tilde{h}_\ell^{(1)}(ka_2) & \tilde{h}_\ell^{(2)}(ka_2) \end{bmatrix}. \quad (76)$$

Note that these are respectively identical with (14) and (15), i.e., $\mathbf{K}_{pq}^E = \mathbf{K}_{pq}$ and $\mathbf{L}^E = \mathbf{L}$. Therefore, as far as the study of the spectral singularities are concerned, we obtain similar results except that $\nu = \sqrt{5}/2$ is now replaced by ℓ . As we see from (37), this does not influence the parameters of the system. It only changes the mode numbers associated with spectral singularities.

Similarly, for TM modes, we find the following set of boundary conditions.

$$\mathbf{K}_{11}^M \begin{bmatrix} a_{M1} \\ 0 \end{bmatrix} = \mathbf{K}_{12}^M \begin{bmatrix} a_{M2} \\ b_{M2} \end{bmatrix}, \quad \mathbf{K}_{22}^M \begin{bmatrix} a_{M2} \\ b_{M2} \end{bmatrix} = \mathbf{L} \begin{bmatrix} a_{M3} \\ b_{M3} \end{bmatrix}, \quad (77)$$

where, for all $p, q = 1, 2$,

$$\mathbf{K}_{pq}^M := \begin{bmatrix} j_\ell(k_q a_p) & n_\ell(k_q a_p) \\ \frac{\tilde{j}_\ell(k_q a_p)}{n_q^2} & \frac{\tilde{n}_\ell(k_q a_p)}{n_q^2} \end{bmatrix}. \quad (78)$$

As we see the only difference between \mathbf{K}_{pq}^M and \mathbf{K}_{pq} is the appearance of the factor $1/n_q^2$ in the second row of \mathbf{K}_{pq}^M . We have shown by explicit calculation that the presence of these extra $1/n_q^2$ factors does not affect the calculation of spectral singularities except for changing the value of the corresponding mode numbers.

References

- [1] A. Mostafazadeh, “Spectral Singularities of Complex Scattering Potentials and Infinite Reflection and Transmission Coefficients at Real Energies,” *Phys. Rev. Lett.* **102**, 220402 (2009).
- [2] M. A. Naimark, “Investigation of the Spectrum and the expansion in eigenfunctions of a non-selfadjoint differential operator of the second order on a semi-axis,” *Trudy Moscov. Mat. Obsc.* **3**, 181 (1954) in Russian, English translation: *Amer. Math. Soc. Transl. (2)*, **16**, 103 (1960); For a recent review see, G. Sh. Guseinov, “On the concept of spectral singularities,” *Pramana. J. Phys.* **73**, 587 (2009).
- [3] A. Mostafazadeh, “Resonance phenomenon related to spectral singularities, complex barrier potential, and resonating waveguides,” *Phys. Rev. A* **80**, 032711 (2009).
- [4] Z. Ahmed, “Zero width resonance (spectral singularity) in a complex PT-symmetric potential,” *J. Phys. A* **42**, 472005 (2009).
- [5] S. Longhi, “Spectral singularities in a non-Hermitian Friedrichs-Fano-Anderson model,” *Phys. Rev. B* **80**, 165125 (2009) and “Spectral singularities and Bragg scattering in complex crystals,” *Phys. Rev. A* **81**, 022102 (2010).
- [6] A. A. Andrianov, F. Cannata, and A. V. Sokolov, “Spectral singularities for non-Hermitian one-dimensional Hamiltonians: Puzzles with resolution of identity,” *J. Math. Phys.* **51**, 052104 (2010).
- [7] S. Longhi, “Backward lasing yields a perfect absorber,” *Physics* **3**, 61 (2010); “PT-symmetric laser absorber,” *Phys. Rev. A* **82**, 031801 (2010) and “Coherent perfect absorption in a homogeneously broadened two-level medium,” *Phys. Rev. A* **83**, 055804 (2011).
- [8] A. Mostafazadeh, “Optical spectral singularities as threshold resonances,” *Phys. Rev. A* **83**, 045801 (2011).
- [9] A. Mostafazadeh, “Semiclassical Analysis of Spectral Singularities and Their Applications in Optics,” *Phys. Rev. A* **84**, 023809 (2011).
- [10] A. Mostafazadeh, “Spectral singularities of a general point interaction,” *J. Phys. A* **44**, 375302 (2011).
- [11] A. Mostafazadeh and M. Sarisaman, “Spectral Singularities of a Complex Spherical Barrier Potential and Their Optical Realization,” *Phys. Lett. A* **375**, 3387 (2011).
- [12] B. F. Samsonov, “Scattering cross-section resonance originating from a spectral singularity,” *J. Phys. A* **44**, 392001 (2011).
- [13] Y. D. Chong, L. Ge, H. Cao, and A. D. Stone, “Coherent Perfect Absorbers: Time-Reversed Lasers,” *Phys. Rev. Lett.* **105**, 053901 (2010); W. Wan, Y. Chong, L. Ge, H. Noh, A. D. Stone, and H. Cao, “Time-Reversed Lasing and Interferometric Control of Absorption,” *Science* **331**, 889 (2011); Y. D. Chong, L. Ge, and A. D. Stone, “PT-Symmetry Breaking and Laser-Absorber Modes in Optical Scattering Systems,” *Phys. Rev. Lett.* **106**, 093902 (2011); S. Longhi, “PT-symmetric laser absorber,” *Phys. Rev. A* **82**, 031801 (2010), “Coherent perfect absorption in a homogeneously broadened two-level medium,” *Phys. Rev. A* **83**, 055804 (2011), and “Time-Reversed Optical Parametric Oscillation,” *Phys. Rev. Lett.* **107**, 033901 (2011); L. Ge, Y. D. Chong, S. Rotter, H. E. Türeci, and A. D. Stone, “Unconventional modes in lasers with spatially varying gain and loss,” *Phys. Rev. A* **84**, 023820 (2011).

- [14] N. G. Alexopoulos, and N. K. Uzunoglu, “Electromagnetic scattering from active objects: invisible scatterers,” *Appl. Opt.*, **17**, 235 (1978); M. Kerker, “Electromagnetic scattering from active objects,” *Appl. Opt.* **17**, 3337 (1978); R. E. Benner, P. W. Barber, J. F. Owen, and R. K. Chang, “Observation of Structure Resonances in the Fluorescence Spectra from Microspheres,” *Phys. Rev. Lett.* **44**, 475 (1980); H. C. van de Hulst, *Light Scattering by Small Particles*, Dover Publications, New York, 1981; C. F. Bohren, and D. R. Huffman, *Absorption and Scattering of Light by Small Particles*, John Wiley & Sons, New York, 1983; V. Sandoghdar, F. Treussart, J. Hare, V. Lefèvre-Seguin, J. M. Raimond, and S. Haroche, “Very low threshold whispering-gallery-mode microsphere laser,” *Phys. Rev. A* **54**, R1777 (1996); K. Sasaki, H. Fujiwara, and H. Masuhara, “Photon tunneling from an optically manipulated microsphere to a surface by lasing spectral analysis,” *Appl. Phys. Lett.* **70**, 2647 (1997); M. L. Gorodetsky and V. S. Ilchenko, “Optical microsphere resonators: optimal coupling to high-Q whispering-gallery modes,” *J. Opt. Soc. Am. B* **16**, 147 (1999); T. Takahashi, K. Fujiwara, S. Matsuo, and H. Misawa, “Excitation energy transfer between dye molecules in lasing microparticles,” *J. Photochem. Photobiol. A* **120**, 135 (1999); W. von Klitzing, R. Long, V. S. Ilchenko, J. Hare, and V. Lefèvre-Seguin, “Tunable whispering gallery modes for spectroscopy and CQED experiments,” *New J. Phys.* **3**, 14.1 (2001); K. J. Vahala, “Optical microcavities,” *Nature*, **424**, 839 (2003).
- [15] A. B. Matsko, A. A. Savchenko, D. Stekalov, V. S. Ilchenko, and L. Maleki, “Review of Applications of Whispering-Gallery Mode Resonators in Photonics and Nonlinear Optics,” IPN Progress Report **42162**, 1 (2005); A. B. Matsko and V. S. Ilchenko, “Optical resonators with whispering-gallery modes-part I: Basics,” *IEEE J. Sel. Topics Quantum Electron.* **12**, 3 (2006).
- [16] M. L. Gorodetsky and V. S. Ilchenko, “Optical microsphere resonators: optimal coupling to high-Q whispering-gallery modes,” *J. Opt. Soc. Am. B* **16**, 147 (1999); R. Sandberg, K. Mølhave, A. Boisen and W. Svendsen, “Effect of gold coating on the Q-factor of a resonant cantilever,” *J. Micromech. Microeng.* **15**, 2249 (2005); D. Eroglu, “Quality Factor Enhancement of Lateral Microresonators in Liquid Media by Hydrophobic Coating,” *Journal of Microelectromechanical Systems*, **20**, 1068 (2011).
- [17] J. D. Jackson, *Classical Electrodynamics*, Wiley & Sons, New York, 1975.
- [18] W. T. Silfvast, *Laser Fundamentals*, Cambridge University Press, Cambridge, 1996.
- [19] A. Y. Nooraldeen, M Palanichant, and P. K. Palanisamy, “Influence of Solvents Polarity on NLO Properties of Fluorone Dye,” *Int. J. Nonlinear Science* **7**, 290 (2009).
- [20] Shibata S., Ashida S., Segawa H. and Yano T., “Coated microsphere as spherical cavity Raman laser,” *J. Sol-Gel Sci. Technol.*, **40** (2006) 379-384.
- [21] Y. Arai, T. Yano, and S. Shibata, “High refractive-index microspheres of optical cavity structure,” *Appl. Phys. Lett.* **82**, 3173 (2003).
- [22] V. V. Datsuyk, S. Juodkazis, and H. Misawa, “Properties of a laser based on evanescent-wave amplification,” *J. Opt. Soc. Am. B* **22**, 1471 (2005); V. R. Dantham and P. B. Bisht, “High-Q whispering gallery modes of doped and coated single microspheres and their effect on radiative rate,” *J. Opt. Soc. Am. B* **26**, 290 (2009); A. M. Beltaos and A. Meldrum, “Whispering gallery modes in silicon-nanocrystal-coated silica microspheres,” *J. Luminescence*, **126**, 607 (2007); Y. F. Xiao, C. L. Zou, B. B. Li, Y. Li, C. L. Dong, Z. F. Han, and Q. Gong, “High-Q exterior whispering-gallery modes in a metal-coated microresonator,” *Phys. Rev. Lett.* **105**, 153902 (2010).